Computers in Biology and Medicine 197 (2025) 111041

Contents lists available at ScienceDirect

Computers in Biology and Medicine

journal homepage: www.elsevier.com/locate/compbiomed

Muti-band Morlet mutual information functional connectivity for classifying Alzheimer's disease and frontotemporal dementia with a deep learning technique

Mingkan Shen [a,b,c,*], Peng Wen [a], Bo Song [d], Yan Li [e]

[a] School of Engineering, University of Southern Queensland, Toowoomba, Australia
[b] Neurosciences Centre, Mater Hospital, South Brisbane, Australia
[c] Mater Research Institute, University of Queensland, South Brisbane, Australia
[d] School of Engineering, University of Southern Queensland, Springfield, Australia
[e] School of Mathematics, Physics and Computing, University of Southern Queensland, Toowoomba, Australia

ARTICLE INFO

Keywords:
AD
FTD
EEG
MMMIFC
3D-CNN
Default mode network
Graph theory

ABSTRACT

Accurate differentiation of Alzheimer's disease (AD), frontotemporal dementia (FTD), and healthy control (HC) is critical for early diagnosis and intervention of brain disorders. This study introduces a deep learning framework that leverages electroencephalography (EEG)-derived multiband functional connectivity (FC) features. Multiband Morlet wavelet mutual information (MMMIFC) was utilized to generate high-resolution FC matrices across 1–20 Hz, which were subsequently processed by a 3D convolutional neural network (3D-CNN) based on a modified VGG architecture. The proposed model achieved classification accuracies of 90.77 % for AD vs HC and 90.38 % for FTD vs HC, with sensitivity and specificity of 88.89 % and 93.10 % for AD vs HC, and 86.96 % and 93.10 % for FTD vs HC, respectively. Beyond classification performance, the analysis identified distinct EEG-based biomarkers within the default mode network. In AD analysis, global efficiency, diffusion efficiency, and clustering coefficient were consistently reduced in the delta and theta bands, reflecting disrupted low-frequency network integration and the theta band presents the most prominent group differences between AD and HC. In FTD analysis, graph theory metrics were also reduced in the delta and theta bands, with the delta band showing the most pronounced group differences compared to HC.

1. Introduction

Alzheimer's disease (AD) is the most prevalent neurodegenerative disorder worldwide, affecting millions of individuals and accounting for most dementia cases [1,2]. Characterized by progressive cognitive decline, especially memory impairment, AD is associated with neuronal loss and abnormal accumulation of β-amyloid plaques and neurofibrillary tangles in the brain. Despite advances in neuroimaging and cerebrospinal fluid biomarkers, early and non-invasive diagnosis remains a significant clinical challenge [3]. Electroencephalography (EEG), as a low-cost and accessible neurophysiological tool, has shown promise in detecting AD related brain changes and monitoring disease progression through alterations in neural oscillations and connectivity patterns [4].

Frontotemporal dementia (FTD) represents a clinically and pathologically heterogeneous group of neurodegenerative disorders primarily affecting the frontal and temporal lobes, leading to prominent changes in behaviour, language, and executive function [5,6]. The pathological hallmarks of FTD differ substantially from those of AD, involving distinct proteinopathies and neurodegenerative processes [7]. Diagnosis of FTD relies heavily on clinical assessment complemented by neuroimaging and, in some cases, neuropathological confirmation, with a notable lack of specific biomarkers for early detection [8]. While EEG studies in FTD are relatively limited, emerging evidence suggests that analyses of EEG functional connectivity (FC) may uncover disease-specific neural network disruptions relevant to FTD pathology [9].

EEG signals are inherently non-stationary and exhibit rich spectral-temporal dynamics. Time-frequency analysis techniques, such as short-time Fourier transform (STFT), wavelets transform, and empirical mode decomposition (EMD), have been widely employed to decompose EEG signals into temporally localized frequency components. These

* Corresponding author. School of Engineering, University of Southern Queensland, Toowoomba, Australia.
E-mail address: Mingkan.Shen@unisq.edu.au (M. Shen).

https://doi.org/10.1016/j.compbiomed.2025.111041
Received 18 June 2025; Received in revised form 16 August 2025; Accepted 30 August 2025
Available online 5 September 2025

approaches enable detailed examination of brain rhythms across canonical frequency bands with delta, theta, alpha, beta, and gamma bands which are known to be affected in various neurological disorders. Time-frequency analysis has been widely applied in studying neurodegenerative diseases such as AD and FTD. Compared to healthy control (HC) subjects, both AD and FTD patients exhibit notable differences in brain oscillatory activity across various frequency bands, reflecting underlying pathological changes [10,11]. However, most existing approaches adopt relatively coarse frequency ranges, which may overlook subtle disease-related oscillatory alterations. Such coarse segmentation can mask narrow-band abnormalities that are critical for differentiating between disease phenotypes or stages. Higher-resolution frequency analysis has the potential to reveal fine-grained changes in specific sub-bands that are otherwise averaged out, capturing early pathological signatures and enabling more precise mapping of disease-related neural dynamics. This makes time–frequency analysis a valuable tool for characterizing disease-related alterations in brain dynamics, particularly when coupled with methods capable of leveraging multi-band information for diagnostic purposes.

Complex brain network analysis provides a comprehensive framework for studying the organization of brain by modelling it as a network of nodes and edges, where nodes represent brain regions or electrodes, and edges denote the interactions between them [12]. FC analysis and effective connectivity (EC) analysis have been widely employed to explore the neural substrates of cognitive processes and to identify disruptions associated with neurodegenerative diseases such as AD and FTD [13,14]. Alterations in the Default Mode Network (DMN) have been consistently reported in both AD and FTD, with disruptions in key hubs such as the posterior cingulate cortex, medial prefrontal cortex, and inferior parietal lobule linked to cognitive decline [15,16]. Although the present study focuses on whole-brain FC patterns, the proposed framework enables post-hoc interpretability analyses that can localize such network-level alterations, including DMN connectivity changes, thereby facilitating mechanistic insights into disease-specific network dysfunctions.

Artificial intelligence techniques have become increasingly vital in the analysis of EEG data, particularly for the early detection and classification of neurodegenerative diseases. Machine learning (ML) and deep learning (DL) methods enable the extraction of complex patterns from high-dimensional EEG signals, facilitating improved diagnostic accuracy beyond traditional clinical assessments [17,18]. These approaches leverage automated feature learning, reducing reliance on handcrafted features and enabling the integration of temporal, spectral, and spatial information inherent in EEG recordings [18]. In this study, a multi-band, multi-modal interpretable functional connectivity (MMMIFC) framework integrated with a three-dimensional convolutional neural network (3D-CNN) is introduced. EEG signals are decomposed into 19 narrow frequency bands spanning 1–20 Hz, each producing a 19×19 FC matrix based on 19 EEG channels. Stacking these matrices yields a $19 \times 19 \times 19$ spectral–spatial representation, enabling high-resolution frequency-band analysis and joint spectral–spatial–temporal feature learning. This design advances beyond conventional EEG-based methods by capturing fine-grained connectivity patterns and supporting post-hoc identification of interpretable biomarkers.

The remainder of this paper is organized as follows. The next section, *'State of the Art'*, reviewed relevant literature on EEG-based detection for AD and FTD, emphasizing the biomarkers of AD and FTD as well. In *'Methodology'*, the proposed multi-band time–frequency functional connectivity framework is described, along with the data collection, signal pre-processing pipeline and the deep learning strategy adopted. The *'Results and Comparison'* section reported the classification performance and biomarker patterns identified across experimental settings and compared with the related works in the same dataset. The subsequent *'Discussion'* section explored frequency-dependent brain dynamics in AD and FTD, emphasizing DMN related alterations, time-varying connectivity patterns, and the methodological insights and limitations of this study. The *'Conclusion'* concluded the paper. The experiments were conducted on a system equipped with an Intel i7-13700F CPU, 64 GB of memory, and an NVIDIA RTX 4070 Ti GPU.

2. State of the art

Broadly, EEG-based studies in the context of AD and FTD can be grouped into several methodological categories. One major focus is on signal processing techniques that extract features from specific frequency bands such as delta, theta, alpha, beta, and gamma bands to characterize alterations in brain rhythms associated with cognitive impairment. These features, which often include power spectral density, entropy measures, and time-frequency representations, have been extensively investigated in studies aiming to delineate the electrophysiological signatures of AD and FTD. In parallel, another line of research explores the brain connectivity patterns by constructing inter-regional relationships from EEG recordings. FC refers to statistical dependencies between signals from different brain regions, while EC captures directional influences and causal interactions. Both FC and EC provide complementary perspectives on large-scale brain network organization and have been increasingly used to understand network-level dysfunction in disorders such as AD and FTD. The related works were summarized as follows.

Miltiadous et al. extracted Relative Band Power (RBP) features across five EEG frequency bands using the Welch method and applied them to machine learning classifiers to distinguish AD, FTD, and HC [19]. Comparing several ML methods, they found the Random Forest (RF) model achieved the highest classification accuracies of 77.01 % for AD vs HC and 72.01 % for FTD vs HC, supporting the diagnostic potential of EEG-based RBP features. In the same year, Miltiadous et al. enhanced the Spectral coherence connectivity (SCC) method based on RBP features and used the DICE-net deep learning method to represent the ML methods [20]. This improved architecture achieved higher accuracy with 83.28 % for AD vs HC and 74.96 % for FTD vs HC which demonstrates the benefit of deep feature extraction in EEG-based dementia classification. Zheng et al. introduced the Multi-Threshold Recurrence Rate Plot (MTRRP) technique, which captures nonlinear and temporal EEG dynamics across multiple thresholds [21]. By combining MTRRP features with a support vector machine (SVM) classifier, their method further improved classification performance, achieving accuracies of 87.69 % for AD vs HC and 82.69 % for FTD vs HC. This highlights the importance of incorporating complex temporal patterns in EEG analysis for more accurate dementia differentiation. Building on this work, Zheng et al. further explored advanced EEG feature extraction by time-frequency domain FC measures with SVM classifiers, demonstrating the continued enhancement of diagnostic accuracy for both AD and FTD [11]. Their latest model achieved impressive performance with an accuracy of 95.38 %, sensitivity of 94.4 %, and specificity of 96.6 % for AD vs HC classification, and an accuracy of 81.54 %, sensitivity of 86.2 %, and specificity of 77.8 % for FTD vs HC classification. AlSharabi et al. developed an EEG-based clinical decision support system for early AD using EMD and DL technique [22]. By applying EMD to extract features from resting-state EEG signals and evaluating several AI classifiers, their approach achieved high diagnostic performance via Convolutional Neural Network (CNN) model, with classification accuracies of 94.8 %, effectively distinguishing between neurotypical individuals and patients with mild or moderate AD. Lal et al., proposed an optimized ML framework that used Singular Value Decomposition (SVD) entropy for feature extraction, and K-Nearest Neighbours (KNN) for classification [23]. The model achieved high classification accuracies: 93 % for AD vs HC, 92.5 % for FTD vs HC, and 91 % for AD vs FTD. The study by Zheng et al. proposed an integrated approach using spectral, complexity, and synchronization features extracted from resting-state EEG signals to distinguish AD from HC [24]. The RF model provided the best result with 95.86 % accuracy, demonstrating that combining multiple EEG

feature types significantly improves diagnostic accuracy for AD. Ma et al. applied the Phase-based Connectivity Index (PHI) with an SVM to EEG data for dementia classification, achieving an impressive 96.6 % accuracy specifically in distinguishing AD from FTD [25]. This result highlights the strong potential of their method for accurate differential diagnosis between these two dementia subtypes. Wang et al. reported an improved Artificial Fish Swarm–Genetic Algorithm (AFS–GA) hybrid method for feature selection from EEG signals to automatically detect AD [26]. They extracted geometric and entropy-based features using a Second-Order Difference Plot (SODP) and applied the hybrid IAFS–GA to optimize feature selection, achieving a classification accuracy of 93.53 %, sensitivity of 98.74 %, and specificity of 98.25 % with a Naive Bayes classifier. This approach demonstrates strong potential for reliable early AD diagnosis based on EEG data.

While many studies have focused on combining EEG signal processing with ML & DL technique to improve diagnostic accuracy, research that emphasizes the extraction and interpretation of discriminative biomarkers remains equally important for understanding the underlying neurophysiological changes in AD and FTD.

In the study by Vicchietti et al., the authors applied six computational time-series analysis methods including wavelet coherence, fractal dimension, quadratic entropy, wavelet energy, quantile graphs, and visibility graphs on raw and wavelet-filtered EEG signals across delta, theta, alpha, and beta frequency bands [27]. The results showed that wavelet coherence in the alpha and beta bands was significantly reduced in AD patients, indicating disrupted functional connectivity. Quantile graph complexity and visibility graph connectivity were also lower in AD subjects, particularly in the delta and theta bands, reflecting simplified brain dynamics. Furthermore, fractal dimension and quadratic entropy exhibited consistent reductions across multiple bands, suggesting a loss of signal complexity and variability in AD. Wavelet energy was notably decreased in the alpha band in AD, highlighting diminished neuronal synchronization. These findings underscore the value of frequency-specific EEG biomarkers in characterizing the neural alterations associated with AD.

Ranjan and Kumar introduced a novel method employing Crossplot Transition Entropy (CPTE) to analyse resting-state EEG data from patients with AD and FTD [28]. The study constructed FC to assess differences in network organization between the two groups. Key findings revealed that FTD patients exhibited higher connectivity measures in specifically clustering coefficient, subgraph centrality, and eigenvector centrality particularly in the delta, theta, and gamma frequency bands. The CPTE-based network parameters achieved a classification accuracy of 87.58 % in distinguishing FTD from AD, with the gamma band yielding the highest accuracy at 92.87 %. These results suggest that CPTE-derived EEG network metrics can serve as potential biomarkers for differentiating FTD from AD.

Al-Ezzi et al. applied Partial Directed Coherence (PDC) to 21-channel EEG recordings of cognitively healthy older adults stratified by CSF Aβ/tau ratios, and found reduced temporal connectivity alongside increased frontal connectivity in the pathological group [29]. These connectivity alterations were associated with neuropsychological measures, MRI volumetrics, and HRV, suggesting that EC can reveal early-stage network changes in preclinical AD.

The MMMIFC method, originally developed for EEG-based detection of schizophrenia and alcoholism, has shown strong performance in our previous studies [30,31]. In the present work, this method is adapted for the classification of EEG signals in AD and FTD. The framework demonstrates not only competitive classification performance but also the ability to extract informative biomarkers relevant to underlying neurophysiological mechanisms.

3. Methodology

Fig. 1 presents an overview of the proposed analytical pipeline, which is organized into four key modules: data acquisition, signal preprocessing, extraction of brain network features via MMMIFC, and classification using a 3D-CNN architecture inspired by VGG. This structured framework facilitates the transformation of raw EEG recordings into high-level representations of functional brain connectivity, which are then utilized for distinguishing among clinical conditions. The following sections describe each processing stage in detail.

3.1. Data collection

The resting-state eyes-closed EEG dataset used in this study was originally collected by Miltiadous et al. and is publicly available on the OpenNeuro platform (https://openneuro.org/datasets/ds004504/versions/1.0.2) [19]. The recordings were acquired at the 2nd Department of Neurology, AHEPA General Hospital, Thessaloniki, Greece. This dataset includes 88 participants: 36 diagnosed with AD, 23 with FTD, and 29 HC. Cognitive function was assessed via the Mini-Mental State Examination (MMSE), where lower scores indicate more severe impairment. The median disease duration for patients was 25 months (IQR: 24–28.5). Diagnoses followed clinical criteria outlined in DSM and ICD guidelines.

EEG signals were recorded using a Nihon Kohden EEG-2100 system, employing 19 scalp electrodes positioned according to the international 10–20 system: Fp1, Fp2, F7, F3, Fz, F4, F8, T3, C3, Cz, C4, T4, T5, P3, Pz, P4, T6, O1, and O2. Two reference electrodes (A1 and A2) were placed on the mastoids for impedance monitoring. Prior to recording, electrode impedance was ensured to be below 5 kΩ. Participants were seated comfortably with eyes closed during approximately 12–14 min of recording. Data were sampled at 500 Hz, with sensitivity set at 10 μV/mm, a time constant of 0.3 s, and a high-frequency filter at 70 Hz.

3.2. Pre-processing

EEG data preprocessing involved several key steps. First, signals were bandpass filtered between 0.5 and 45 Hz using a Butterworth filter and referenced to the average of mastoid electrodes (A1 and A2). Artifact subspace reconstruction within EEGLAB toolbox based on MATLAB

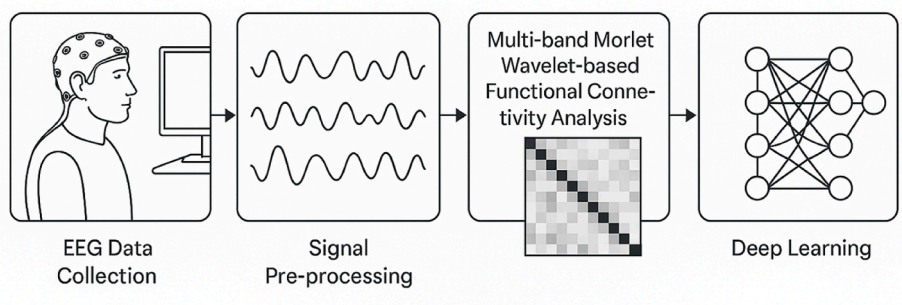

Fig. 1. The overview of the proposed methodology to detect AD and FTD.

was applied next, removing segments with excessive noise defined by a 0.5-s sliding window exceeding a standard deviation (SD) threshold of 17. Then, Independent Component Analysis (ICA) via the *'RunICA'* algorithm separated the 19 channels into independent components. Components classified as ocular or jaw artifacts by the *'ICLabel'* tool were excluded. Although recordings were obtained during eyes-closed resting states, residual artifacts related to eye and jaw movements were detected and eliminated through this process.

To capture temporal variability in brain connectivity, dynamic functional connectivity was computed using a sliding window approach. A window size of 30 s was applied to the cleaned EEG signals, with connectivity calculated every 5 s, enabling the analysis of connectivity fluctuations over time.

3.3. Multi-band Morlet mutual information functional connectivity

To quantify nonlinear and frequency-specific functional connectivity between EEG channels, a method based on mutual information (MI) of time-frequency power features derived using Morlet wavelet transform (MWT) was employed. This measure is referred to as MMMIFC.

3.3.1. Time-frequency power estimation

To extract dynamic spectral features from the EEG data, a time-frequency analysis was performed using the MWT. The EEG signals were segmented into 30-s epochs, and each epoch was analysed independently. The analysis covered the frequency range from 1 Hz to 20 Hz, which captures the delta, theta, alpha, and low beta bands commonly associated with cognitive and pathological brain states.

For each central frequency *'f_{cr}'*, a complex Morlet wavelet was constructed with a fixed time-frequency resolution ratio ($f_c/\ \sigma_f\ =\ 7$), ensuring an optimal balance between temporal localization and frequency precision. The wavelet was defined in equation (1).

$$\psi(t) = A \cdot e^{\left(-\frac{t^2}{2\sigma_t^2}\right)} \cdot e^{2\pi i f_c t} \tag{1}$$

where $\sigma_f\ = f_c/7$, $\sigma_t\ = 1/(2\pi\sigma_f)$, and '$A$' is a normalization factor. The wavelet was truncated to a finite support of $\pm 3.3\ \sigma_t$ to maintain numerical efficiency while preserving most of the signal energy.

The signal was convolved with each wavelet to obtain the time-frequency representation. The absolute value of the resulting complex output was used to compute the power distribution over time and frequency. This approach enables the visualization of transient oscillatory activities and their evolution, which is critical for studying dynamic functional connectivity. In this experiment, the transform is applied across a frequency range of 1–20 Hz with 1 Hz resolution (i.e., 1–2 Hz, 2–3 Hz, …, 19–20 Hz), using a wavelet width parameter of 1 to balance time and frequency resolution.

For each frequency band *'f'*, the average time-frequency power is computed for each channel in equation (2)

$$P_C(f) = mean\left(\left|W_f(x_c(t))\right|^2\right) \tag{2}$$

where *'$W_f(x_c(t))$'* denotes the MWT at frequency *'f'*, *'$x_c(t)$'* and is the time series of channel *'c'*.

3.3.2. Mutual information-based connectivity estimation

For each frequency band, the mutual information is computed between all pairs of channels based on their averaged power values. The mutual information between two random variables *'P_i'* and *'P_j'* is calculated in equation (3)

$$MI(P_i, P_j) = \sum_{x,y} p_{ij}(x,y) \log\left(\frac{p_{ij}(x,y)}{p_i(x)p_j(y)}\right) \tag{3}$$

where *'$p_i(x)$'* and *'$p_j(y)$'* are the marginal probability density functions, and *'$p_{ij}(x,y)$'* is the corresponding joint distribution.

To account for varying marginal entropies and enhance comparability across channel pairs, the mutual information values are normalized by self-information, the formula is described in equation (4)

$$H^{(f)}(i,j) = \frac{MI(P_i, P_j)}{MI(P_i, P_i)} \tag{4}$$

The resulting matrix *'$H^{(f)} \in R^{C\times C}$'* is symmetrized to form the final frequency-specific connectivity matrix shown in equation (5)

$$\mathrm{MMMIFC} = \frac{H^{(f)} + \left(H^{(f)}\right)'}{2} \tag{5}$$

This computation is repeated across all selected frequency bands to obtain a three-dimensional tensor that *'$T \in R^{C\times C\times F}$'* where *'$F = 19$'* is the number of the frequency bands.

To remove trivial and redundant connections, diagonal elements and unity values in each matrix *'$MMMIFC^{(f)}$'* are set to zero. The final tensor *'T'* reflects nonlinear, frequency-resolved functional dependencies between EEG channels and serves as the input for deep learning analysis and the detail is shown in Fig. 2.

3.4. Classification through 3D VGG-inspired CNN technique

In this study, the input to the model is a three-dimensional MMMIFC matrix with dimensions 19 × 19 × 19, representing large-scale interactions within the brain. In the context of complex brain network analysis, such matrices are interpreted as adjacency matrices that encode pairwise relationships between brain regions across multiple dimensions. Structurally, this forms a brain graph where each node denotes a brain region, and the edge weights capture the strength of inter-regional communication. These brain graphs provide a compact and comprehensive representation of global brain dynamics. Unlike raw EEG signals, which are time-series data recorded from individual electrodes, FC matrices capture the topological organization of functional connections across the whole brain. This makes them particularly suitable for studying complex neurological disorders such as AD and FTD, where abnormal network connectivity plays a central role (see Table 1).

3.4.1. 3D VGG-inspired CNN model

To effectively capture the spatial dependencies and latent topological features embedded in the MMMIFC matrices, a deep three-dimensional VGG-inspired CNN was designed. The architecture consists of four convolutional blocks, each comprising two 3D convolutional layers with ReLU activations, followed by a 3D max-pooling layer for spatial down-sampling. These sequential blocks enable the extraction of hierarchical features, allowing the network to learn both localized and distributed connectivity patterns inherent to the brain network topology. Following the convolutional layers, the extracted features are flattened and passed through two fully connected layers with ReLU activations and dropout regularization. A final fully connected layer followed by a SoftMax activation outputs the predicted class probabilities. The architecture detail is summarized in Table 2.

3.4.2. Leaving one group out training method

To evaluate the generalization performance of the proposed model, a leaving one group out validation strategy was adopted. Each diagnostic category including AD, FTD, and HC was subdivided into six non-overlapping subject groups, as detailed in Table 3.

For the AD vs HC classification task, in each validation fold, one AD group and one HC group were selected as the test set, while the remaining five AD and five HC groups were used for training. This procedure was repeated six times so that every group pair served as the test set exactly once. The same strategy was applied to the FTD vs HC and AD vs FTD classification tasks. In each fold, 20 % of the training data was randomly allocated as an internal validation set to fine-tune model

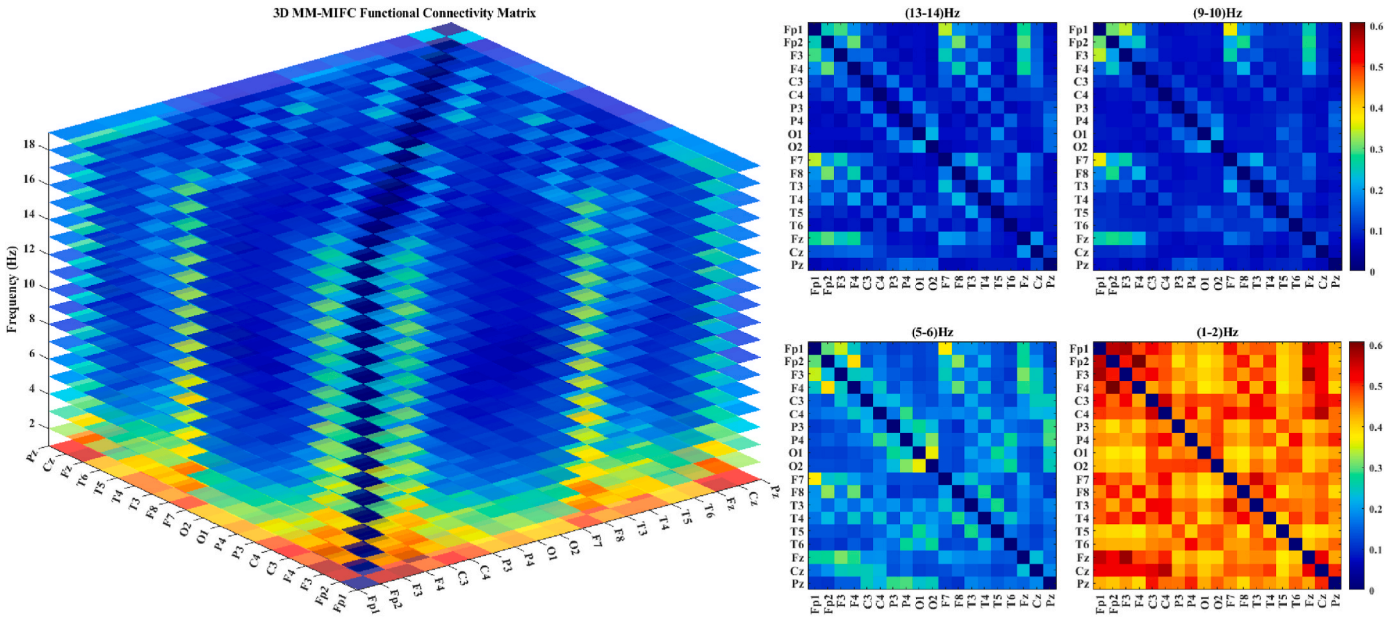

Fig. 2. 3D MMMIFC matrix across frequencies (1–19 Hz) with four representative 2D connectivity matrices at (1–2 Hz), (5–6 Hz), (9–10 Hz) and (13–14 Hz).

Table 1
Summarizes the demographic and clinical data of the participants.

Group	Gender (Male/ Female)	Age (mean ± SD)	MMSE (mean ± SD)	Disease duration (months)
AD	12/24	66.4 ± 7.9	17.75 ± 4.50	25 (24–28.5)
FTD	9/14	63.6 ± 8.2	22.17 ± 8.22	25 (24–28.5)
HC	11/18	67.9 ± 5.4	30.00 ± 5.40	N/A

parameters and monitor overfitting. The validation data were randomly selected from the training set without replacement, and the remaining samples were used for model training. This leaving one group strategy ensures subject-independent validation and allows for robust assessment across group-level variability. Final classification results were averaged across all folds.

3.4.3. *Training configuration selection*

The training configuration was carefully selected to ensure stable convergence and effective feature learning from the high-dimensional 3D functional connectivity data. The model was optimized using the

Table 2
The 3D VGG-inspired CNN architecture used in EEG AD & FTD detection.

Block	Layer	Input Size	Output Size	Hyperparameters
Input	3D imaged-data input	19 × 19 × 19 × 1	19 × 19 × 19 × 1	–
Block 1	Convolutional Layer	19 × 19 × 19 × 1	19 × 19 × 19 × 8	Kernel: 3 × 3 × 3, Stride: 1 × 1 × 1, Channels: 8.
	ReLU	19 × 19 × 19 × 8	19 × 19 × 19 × 8	–
	Convolutional Layer	19 × 19 × 19 × 8	19 × 19 × 19 × 8	Kernel: 3 × 3 × 1, Stride: 1 × 1 × 1, Channels: 8.
	ReLU	19 × 19 × 19 × 8	19 × 19 × 19 × 8	–
	Max Pooling Layer	19 × 19 × 19 × 8	9 × 9 × 9 × 8	Pool Size: 2 × 2 × 2, Stride: 2 × 2 × 2
Block 2	Convolutional Layer	9 × 9 × 9 × 8	9 × 9 × 9 × 16	Kernel: 3 × 3 × 3, Stride: 1 × 1 × 1, Channels: 16.
	ReLU	9 × 9 × 9 × 16	9 × 9 × 9 × 16	–
	Convolutional Layer	9 × 9 × 9 × 16	9 × 9 × 9 × 16	Kernel: 3 × 3 × 3, Stride: 1 × 1 × 1, Channels: 16.
	ReLU	9 × 9 × 9 × 16	9 × 9 × 9 × 16	–
	Max Pooling Layer	9 × 9 × 9 × 16	4 × 4 × 4 × 16	Pool Size: 2 × 2 × 2, Stride: 2 × 2 × 2
Block 3	Convolutional Layer	4 × 4 × 4 × 16	4 × 4 × 4 × 32	Kernel: 3 × 3 × 3, Stride: 1 × 1 × 1, Channels: 32.
	ReLU	4 × 4 × 4 × 32	4 × 4 × 4 × 32	–
	Convolutional Layer	4 × 4 × 4 × 32	4 × 4 × 4 × 32	Kernel: 3 × 3 × 3, Stride: 1 × 1 × 1, Channels: 32.
	ReLU	4 × 4 × 4 × 32	4 × 4 × 4 × 32	–
	Max Pooling Layer	4 × 4 × 4 × 32	2 × 2 × 2 × 32	Pool Size: 2 × 2 × 2, Stride: 2 × 2 × 2
Block 4	Convolutional Layer	2 × 2 × 2 × 32	2 × 2 × 2 × 64	Kernel: 3 × 3 × 3, Stride: 1 × 1 × 1, Channels: 64.
	ReLU	2 × 2 × 2 × 64	2 × 2 × 2 × 64	–
	Convolutional Layer	2 × 2 × 2 × 64	2 × 2 × 2 × 64	Kernel: 3 × 3 × 3, Stride: 1 × 1 × 1, Channels: 64.
	ReLU	2 × 2 × 2 × 64	2 × 2 × 2 × 64	–
	Max Pooling Layer	2 × 2 × 2 × 64	1 × 1 × 1 × 64	Pool Size: 2 × 2 × 2, Stride: 2 × 2 × 2
Fully Connected	Fully Connected Layer	1 × 1 × 1 × 64	1 × 1 × 1 × 128	Channels: 128
	ReLU	1 × 1 × 1 × 128	1 × 1 × 1 × 128	–
	Dropout Layer	1 × 1 × 1 × 128	1 × 1 × 1 × 128	Dropout Rate: 50 %
	Fully Connected Layer	1 × 1 × 1 × 128	1 × 1 × 1 × 128	Channels: 128
	ReLU	1 × 1 × 1 × 128	1 × 1 × 1 × 128	–
	Dropout Layer	1 × 1 × 1 × 128	1 × 1 × 1 × 128	Dropout Rate: 50 %
	Fully Connected Layer	1 × 1 × 1 × 128	1 × 1 × 1 × 2	Output classes: 2
	SoftMax	1 × 1 × 1 × 2	1 × 1 × 1 × 2	
Output	Classification Layer	1 × 1 × 1 × 2	1 × 1 × 1 × 2	–

Table 3
Six-group data for classification.

Group	AD (36 subjects)	FTD (23 subjects)	HC (29 subjects)
Group 1	Sub-001, Sub-002, Sub-003, Sub-004, Sub-005, Sub-006.	Sub-066, Sub-067, Sub-068, Sub-069.	Sub-037, Sub-038, Sub-039, Sub-040, Sub-041.
Group 2	Sub-007, Sub-008, Sub-009, Sub-010, Sub-011, Sub-012.	Sub-070, Sub-071, Sub-072, Sub-073.	Sub-042, Sub-043, Sub-044, Sub-045, Sub-046.
Group 3	Sub-013, Sub-014, Sub-015, Sub-016, Sub-017, Sub-018.	Sub-074, Sub-075, Sub-076, Sub-077.	Sub-047, Sub-048, Sub-049, Sub-050, Sub-051.
Group 4	Sub-019, Sub-020, Sub-021, Sub-022, Sub-023, Sub-024.	Sub-078, Sub-079, Sub-080, Sub-081.	Sub-052, Sub-053, Sub-054, Sub-055, Sub-056.
Group 5	Sub-025, Sub-026, Sub-027, Sub-028, Sub-029, Sub-030.	Sub-082, Sub-083, Sub-084, Sub-085.	Sub-057, Sub-058, Sub-059, Sub-060, Sub-061.
Group 6	Sub-031, Sub-032, Sub-033, Sub-034, Sub-035, Sub-036.	Sub-086, Sub-087, Sub-088.	Sub-062, Sub-063, Sub-064, Sub-065.

Adam algorithm, a stochastic gradient-based optimizer known for its computational efficiency and ability to handle sparse gradients and non-stationary objectives. An initial learning rate of 1×10^{-4} was used, which is commonly recommended when employing Adam to prevent overshooting in the early stages of training, particularly in deep networks with complex spatial structures.

The model was trained for a maximum of 20 epochs, providing sufficient iterations for convergence while avoiding excessive overfitting. A mini-batch size of 32 was used to balance memory efficiency and gradient estimation stability. To reduce variance due to data order and promote better generalization, the training data were shuffled at the beginning of each epoch.

To prevent overfitting and encourage model generalization, L2 weight regularization (also known as weight decay) was applied with a regularization factor of 0.0001. This regularization technique penalizes large weights and helps constrain the complexity of the model.

Training and validation processes were executed on a GPU-accelerated environment, which significantly reduced computation time and allowed for real-time visualization of training progress. A training progress plot was generated, displaying metrics such as loss and accuracy curves for both training and validation, aiding in hyperparameter adjustment and training diagnostics. The optimizer of the proposed 3D VGG-spired CNN model in MATLAB 2023B is shown in Fig. 3.

4. Results and Comparison

4.1. Model classification performance

To comprehensively evaluate the classification performance of the proposed method across different diagnostic tasks, confusion matrices were employed to visually represent the model's prediction results on various classes. Confusion matrices provide not only the counts of correct and incorrect predictions but also form the basis for calculating key performance metrics.

In this study, three primary metrics are considered, including accuracy, sensitivity and specificity.

Accuracy indicates the proportion of correctly predicted samples among all tested samples, calculated as:

$$Acc = \frac{TP + TN}{TP + TN + FP + FN} \tag{6}$$

where *'TP'* is true positive and *'TN'* is true negative denote the number of correctly classified positive and negative samples, respectively, while *'FP'* is false positive and *'FN'* is false negative representing misclassified samples.

Sensitivity called recall, measures the model's ability to correctly identify positive samples:

$$Sen = \frac{TP}{TP + FN} \tag{7}$$

Specificity reflects the model's capability to correctly identify negative samples:

$$Spe = \frac{TN}{TN + FP} \tag{8}$$

Fig. 4 illustrates the confusion matrices for three classification tasks, including AD vs HC, FTD vs HC, and AD vs FTD. These matrices facilitate a direct assessment of prediction accuracy and error distribution.

From the confusion matrices, the overall accuracy for the AD vs HC classification reached 90.77 %, with sensitivity and specificity of 88.89 % and 93.10 %, respectively. The FTD vs HC task achieved an accuracy

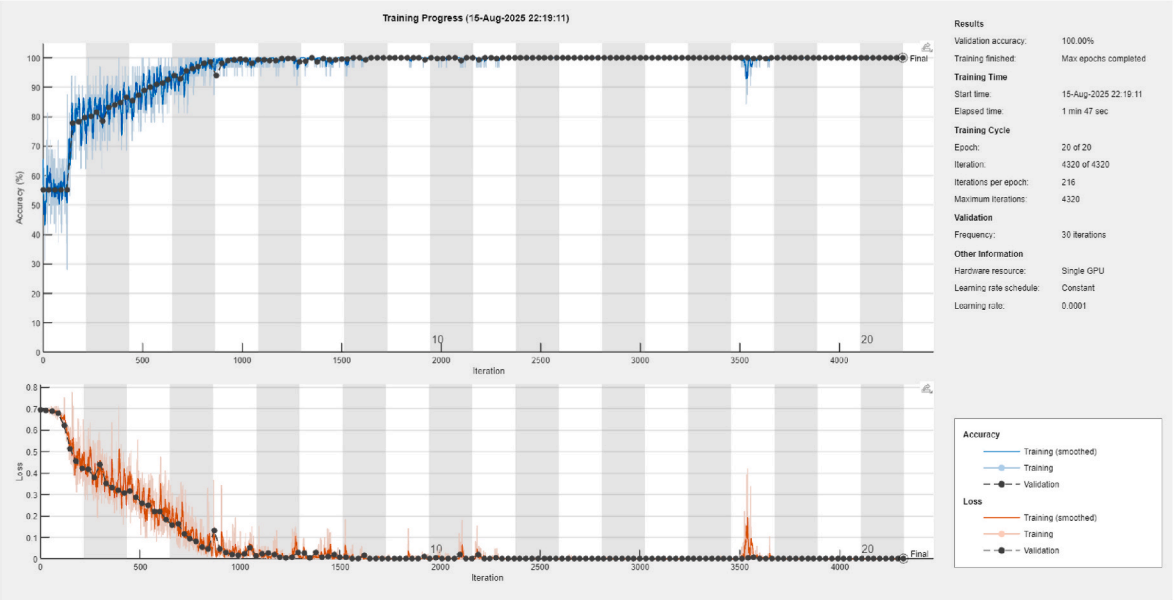

Fig. 3. The optimizer of 3D VGG-spired CNN model.

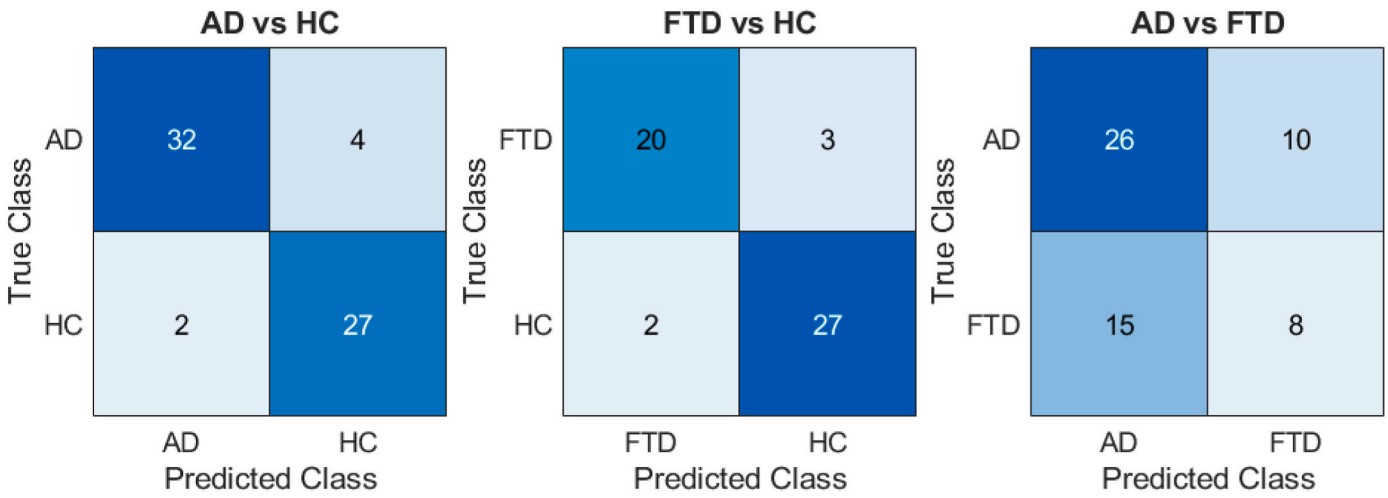

Fig. 4. Confusion matrices of the classification performance among the proposed method.

of 90.38 %, sensitivity of 86.96 %, and specificity of 93.10 %. For the more challenging AD vs FTD classification, the accuracy decreased to 57.63 %, with a sensitivity of 72.22 % and specificity of 34.78 %.

These results demonstrate that the proposed model effectively distinguishes neurodegenerative diseases from HC with high precision. The lower performance in differentiating AD from FTD reflects the overlapping clinical and neurophysiological features between these conditions, indicating the need for further refinement or additional biomarkers to improve discrimination.

4.2. Baseline classifier comparison

In the 3D - CNN framework, the feature representation was organized into a 19 × 19 × 19 (6859) image data format. To assess the robustness and transferability of the MMMIFC features outside a deep learning context, three representative conventional classifiers including SVM, Decision Tree (DT), and KNN were employed for comparative analysis. This baseline evaluation clarifies whether the observed classification gains are attributable mainly to the intrinsic properties of the features or to the neural network architecture. Given the symmetrical nature of the MMMIFC matrix and the fact that self-connections (e.g., Pz to Pz) have constant zero values, only the non-redundant upper-triangular elements were preserved, yielding (19 × 19–19)/2 × 19 = 3249 unique features. The performance outcomes for these three classifiers are reported in Table 4.

Table 4 clearly shows that the proposed deep learning approach outperforms the three conventional machine learning methods in distinguishing both AD from HC and FTD from HC.

4.3. Previous works comparison

To contextualize the current results, a comparison with previous studies employing the same dataset is presented. Table 5 summarizes the reported classification accuracies along with the methodologies utilized in these studies.

Table 5
Comparison with previous work in EEG AD/FTD detection.

Reference	Technique	AD vs HC	FTD vs HC
Miltiadous et al. (2023) [19]	RBP + RF	Acc: 77.01 % Sen: 78.32 % Spe: 80.94 %	Acc: 72.01 % Sen: 72.32 % Spe: 80.94 %
Miltiadous et al. (2023) [20]	RBP, SCC + DICE-net	Acc: 83.28 % Sen: 79.81 % Spe: 87.94 %	Acc: 74.96 % Sen: 60.62 % Spe: 78.63 %
Zheng et al. (2024) [21]	MTRRP + SVM	Acc: 87.69 % Sen: 73.91 % Spe: 89.66 %	Acc: 82.69 % Sen: 73.91 % Spe: 89.66 %
Lal et al. (2024) [23]	SVD entropy + KNN	Acc: 91 % F1-score: 93 %	Acc: 93 % F1-score: 92.5 %
Ma et al. (2024) [25]	PHI + SVM	Acc: 76.92 % Sen: 97.22 % Spe: 51.72 %	Acc: 90.38 % Sen: 78.26 % Spe: 100.00 %
Zheng et al. (2025) [11]	CMI-FC + SVM	Acc: 95.38 % Sen: 94.4 % Spe: 96.6 %	Acc: 81.54 % Sen: 86.2 % Spe: 77.8 %
Proposed method (2025)	MMMI-FC + 3D VGG-inspired CNN	**Acc: 90.77 %** **Sen: 88.89 %** **Spe: 93.10 %**	**Acc: 90.38 %** **Sen: 86.96 %** **Spe: 93.10 %**

Table 4
Comparison with three machine learning methods.

	AD vs HC			FTD vs HC		
Machine & Deep learning methods	Acc	Sen	Spe	Acc	Sen	Spe
DT	84.62 %	83.33 %	86.21 %	84.62 %	82.61 %	86.21 %
SVM	90.14 %	86.11 %	93.10 %	88.46 %	86.96 %	89.66 %
KNN	87.69 %	86.11 %	89.66 %	86.54 %	82.61 %	89.66 %
Proposed method 3D VGG-inspired CNN	90.77 %	88.89 %	93.10 %	90.38 %	86.96 %	93.10 %

Table 5 presents a comparative analysis of the proposed method against several recent approaches in EEG-based detection of AD and FTD. While many prior studies have achieved competitive classification accuracy using various combinations of entropy measures, feature selection techniques, and traditional classifiers such as SVM, KNN, RF, the proposed method of this experiment based on MMMIFC, and a 3D VGG-inspired CNN demonstrates consistently strong performance across both AD and FTD classifications.

Importantly, unlike most earlier methods that focus purely on classification accuracy, the proposed approach leverages FC as a core feature representation. This not only enhances diagnostic performance but also provides neurobiologically interpretable insights, potentially serving as biomarkers for disrupted neural communication in neurodegenerative diseases. FC analysis captures alterations in inter-regional brain dynamics, offering a more physiologically grounded understanding of cognitive impairment, which is crucial for early detection and clinical decision-making.

5. Discussion

5.1. Frequency bands selection

The selection of the 1–20 Hz frequency band was data-driven, based on observations from the time-frequency power spectrum derived using the MWT algorithm. The spectral analysis conducted across the AD, FTD, and HC groups indicated that most of the EEG energy was concentrated in the low-frequency range between 1 Hz and 20 Hz. Corresponding power distribution plots further supported this finding, demonstrating that neural activity within this range exhibited the most prominent fluctuations across all subject groups, as shown in Fig. 5. The data presented in Fig. 5 were extracted from the Pz electrode, which is located near the posterior midline and considered a key node of the DMN which is a brain system critically involved in memory, attention, and self-referential processing. This range spans the delta, theta, alpha, and beta bands, which have been repeatedly implicated in cognitive processing, attention, and neurodegenerative pathology.

This frequency interval encompasses the delta, theta, alpha and beta bands, which have been frequently associated with cognitive processing and neurodegeneration. Prior research has demonstrated that alterations in these frequency bands are characteristic of dementia-related brain changes. Specifically, Chetty et al. reported that AD patients exhibited significantly increased theta power and reduced connectivity in theta and alpha bands, indicating abnormal neural synchronization in these low-frequency ranges [32]. Furthermore, a recent study in proposed by Zheng et al. revealed that AD was associated with prominent reductions in time-frequency functional connectivity within the delta, theta, and alpha bands, particularly in frontal and temporal areas [11]. In addition, Rostamikia et al. systematically compared EEG features of AD and FTD, showing that both conditions presented distinctive patterns of spectral power within low frequency bands [33]. In their work, AD was characterized by elevated delta and theta activity and reduced alpha and beta power, whereas frontotemporal dementia exhibited relatively preserved beta power with different topographical distributions. Focusing the analysis within this frequency range enabled a more targeted investigation of the functional dynamics most relevant to disease mechanisms, while simultaneously minimizing the influence of higher-frequency noise and reducing the dimensionality of the input data.

In the current framework, the 1–20 Hz band is not treated as a single block but is subdivided into 19 contiguous 1 Hz-wide sub-bands. This subdivision produces a distinct functional connectivity matrix for each sub-band, enabling the capture of narrow-band alterations that might be diluted when using broader conventional ranges. By integrating these sub-band matrices into a unified multi-dimensional representation, the method can exploit subtle differences in oscillatory coupling across both frequency and spatial domains. Such granularity supports a more precise characterization of group-specific neural dynamics and provides a richer feature space for the subsequent classification stage.

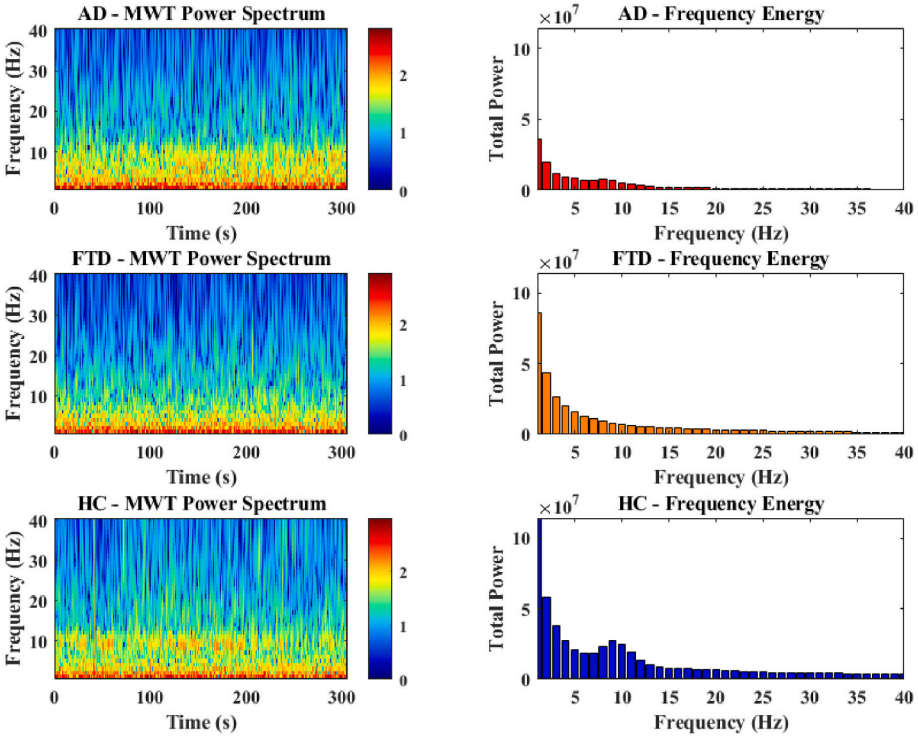

Fig. 5. Mwt power spectrum and frequency energy distribution.

5.2. Exploring information theoretic effective connectivity for AD vs FTD classification

The proposed MMMIFC framework combined with 3D-CNN just achieved an accuracy of 57.63 %, a sensitivity of 72.22 % and specificity of 34.78 % result in distinguishing AD from FTD. To further investigate whether alternative connectivity measures could improve classification performance, seven information-theoretic EC algorithms including Information Geometric Causal Inference (IGCI), Conditional Distribution Similarity Fit (CDS), Regression Error Based Causal Inference (RECI), Additive Noise Model (ANM), Causally Conditioned Entropy (CCE), Directed Information (DI), Transfer Entropy (TE) were evaluated using the same pre-processing procedure. These EC methods were implemented via the PySPI toolbox, and the classification results are summarized in Table 6.

Among these methods, CCE yielded the best performance of Table 5, achieving classification accuracy of 72.88 %, sensitivity of 75.00 % and specificity of 69.57 %, respectively, for the AD vs FTD task. However, for the AD vs HC and FTD vs HC classifications, no performance improvement over the MI-based approach was observed. Nevertheless, the highest accuracy obtained with these EC-based features still falls considerably short of that reported in recent studies employing power spectrum–based features. Acharya et al. proposed one CWT-based spectrogram classification approach using a lightweight EEGConvNeXt network achieved an accuracy of 98.21 %, sensitivity of 98.29 %, specificity of 98.05 % in AD vs FTD discrimination [34]. These results highlight a substantial performance gap between the present EC-based approach and certain power spectrum–oriented reported in the literature.

It should be noted that frequency-domain EC algorithms were not considered in this comparison, as such methods typically require multivariate autoregressive (MVAR) modelling such as Directed Transfer Function (DTF), Directed Coherence (DC), PDC, Granger Causality (GC), Group Delay (GD). This modelling framework differs fundamentally from the MWT-based signal processing approach adopted in this study, making direct comparisons inappropriate. Therefore, the present analysis focuses solely on information-theoretic EC methods applied in the time domain to assess their potential for improving AD vs FTD discrimination.

5.3. Investigations of brain functions across frequency bands

Functional connectivity patterns were examined across four classical EEG frequency bands as delta (1–4 Hz), theta (4–8 Hz), alpha (8–13 Hz), and beta (13–20 Hz) to investigate differences in brain network characteristics among AD, FTD, and HC groups. These frequency bands were selected to capture a broad range of brain oscillatory activity, from slow-wave synchronization to faster rhythms associated with cognitive functions.

Figs. 6 and 7 display the average functional connectivity matrices of AD vs HC and FTD vs HC, respectively, across all four bands. The visualizations reveal that both AD and FTD groups exhibit generally reduced functional connectivity values compared to the HC group, particularly in the lower frequency bands (delta and theta). As the frequency increases toward the alpha and beta bands, the differences in connectivity values between patient groups and controls appear less pronounced. These findings suggest a frequency-dependent attenuation of functional connectivity in AD and FTD, with more evident reductions occurring in slower oscillatory activity.

5.3.1. Definition and electrode mapping of the DMN

DMN is a set of interconnected brain regions that are more active during resting states than during externally directed cognitive tasks [35]. It plays a critical role in internally focused cognitive functions such as autobiographical memory, self-referential thought, and mental simulation. The DMN typically includes the medial prefrontal cortex (PFC), posterior cingulate cortex (PCC), lateral temporal cortex (LTC), and related parts of the occipital cortex (OC).

Alterations in DMN connectivity have been extensively implicated in neurodegenerative diseases. In AD research, numerous f-MRI studies have reported significant disruptions in posterior DMN connectivity, particularly in the PCC and precuneus regions, which are among the earliest affected sites by amyloid pathology reported by Greicius et al. [36]. In addition, Zhou et al. stated that f-MRI research in FTD has revealed dissociable patterns: while AD patients exhibit posterior DMN disconnection, FTD patients tend to show reduced connectivity in the anterior DMN, including the medial PFC and anterior temporal regions [37]. These differential signatures suggest that DMN-based biomarkers may aid in distinguishing dementia subtypes.

To extend these findings, the present study further investigates DMN-related functional connectivity using EEG data. By analysing connectivity patterns among selected DMN-relevant scalp electrodes, we aim to explore whether EEG-based functional alterations in the DMN can differentiate between AD, FTD, and HC. Compared to f-MRI, EEG offers superior temporal resolution and the potential for real-time, low-cost monitoring of brain network dynamics. In this study, 10 EEG channels were selected which were Fp1, Fp2, P3, P4, O1, O2, T3, T4, Cz, and Pz that approximately map to key DMN hubs. These electrodes allow us to probe the anterior, posterior, and lateral subsystems of the DMN from an electrophysiological perspective. Although O1 and O2 are traditionally associated with the occipital lobe and primary visual cortex, recent studies suggest that occipital regions may exhibit functional coupling with posterior DMN hubs, such as the precuneus and posterior cingulate cortex, particularly in resting-state conditions [38,39]. Therefore, O1 and O2 were included in the DMN analysis to extend the spatial coverage of posterior cortical activity and to better capture disease-related disruptions in large-scale network integration. A summary of the anatomical and functional correspondences is provided in Table 7.

5.3.2. Evaluation of brain function in AD and HC

After removing ocular, muscular, and cardiac artifacts with ICA, the cleaned EEG signals were decomposed into delta (1–4 Hz), theta (4–8 Hz), alpha (8–13 Hz), and beta (13–20 Hz) bands using MWT. Pairwise cross-mutual information was then computed among ten electrodes associated with the DMN of Tabel 5 to produce a weighted adjacency matrix $W = w_{ij}$ for each subject and frequency band.

Table 6
Comparison of Classification Results with seven Information Theoretic EC algorithm.

	AD vs HC			FTD vs HC			AD vs FTD		
Connectivity Method	Acc	Sen	Spe	Acc	Sen	Spe	Acc	Sen	Spe
IGCI	76.92 %	72.22 %	82.76 %	71.15 %	60.87 %	79.31 %	54.24 %	55.56 %	52.17 %
CDS	78.46 %	72.22 %	86.21 %	76.92 %	69.57 %	82.76 %	59.32 %	58.33 %	60.87 %
RECI	70.77 %	63.89 %	79.31 %	71.15 %	60.87 %	79.31 %	57.63 %	58.33 %	56.52 %
ANM	86.15 %	83.33 %	89.66 %	84.62 %	78.26 %	89.66 %	67.80 %	72.22 %	60.87 %
CCE	90.77 %	88.89 %	93.10 %	86.54 %	78.26 %	93.10 %	72.88 %	75.00 %	69.57 %
DI	87.69 %	83.33 %	93.10 %	84.62 %	78.26 %	89.66 %	69.49 %	72.22 %	65.22 %
TE	81.54 %	75.00 %	89.66 %	78.85 %	69.57 %	86.21 %	59.32 %	75.00 %	34.78 %
MI	90.77 %	88.89 %	93.10 %	90.38 %	86.96 %	93.10 %	57.63 %	72.22 %	34.78 %

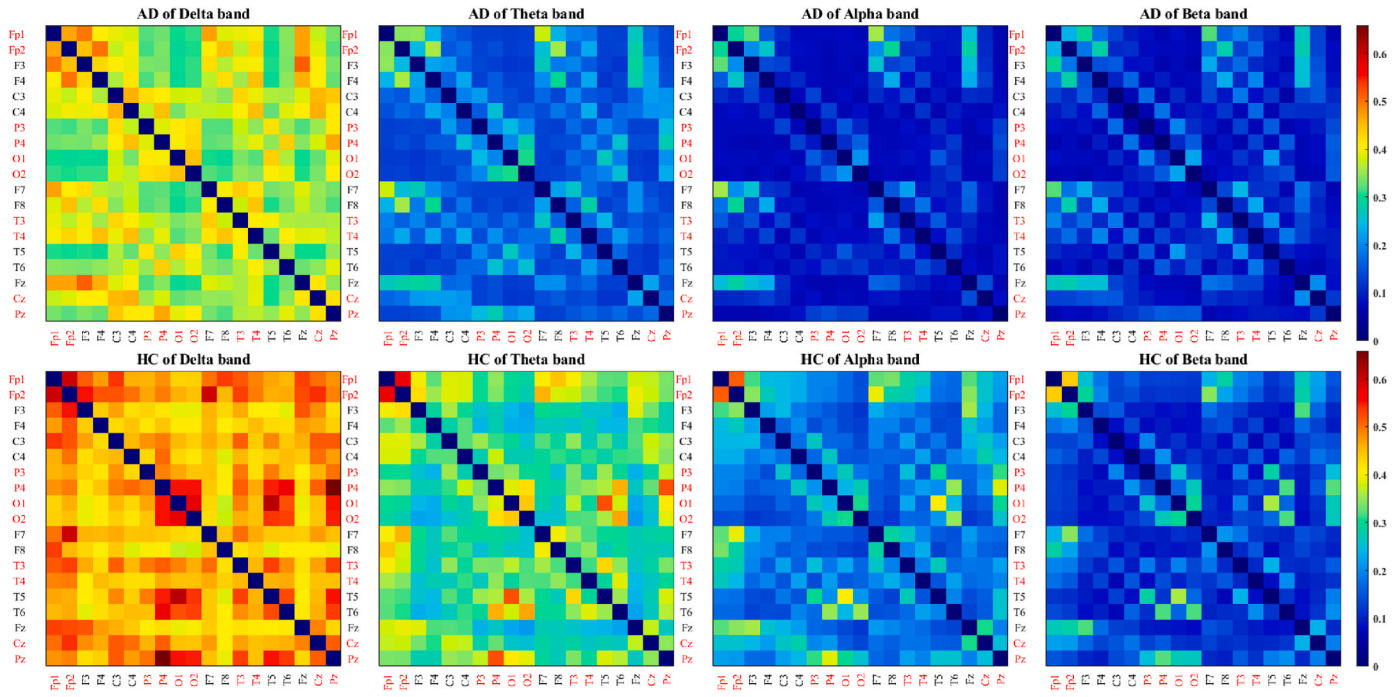

Fig. 6. MMMIFC connectivity matrix of AD and HC in delta, theta, alpha and beta band.

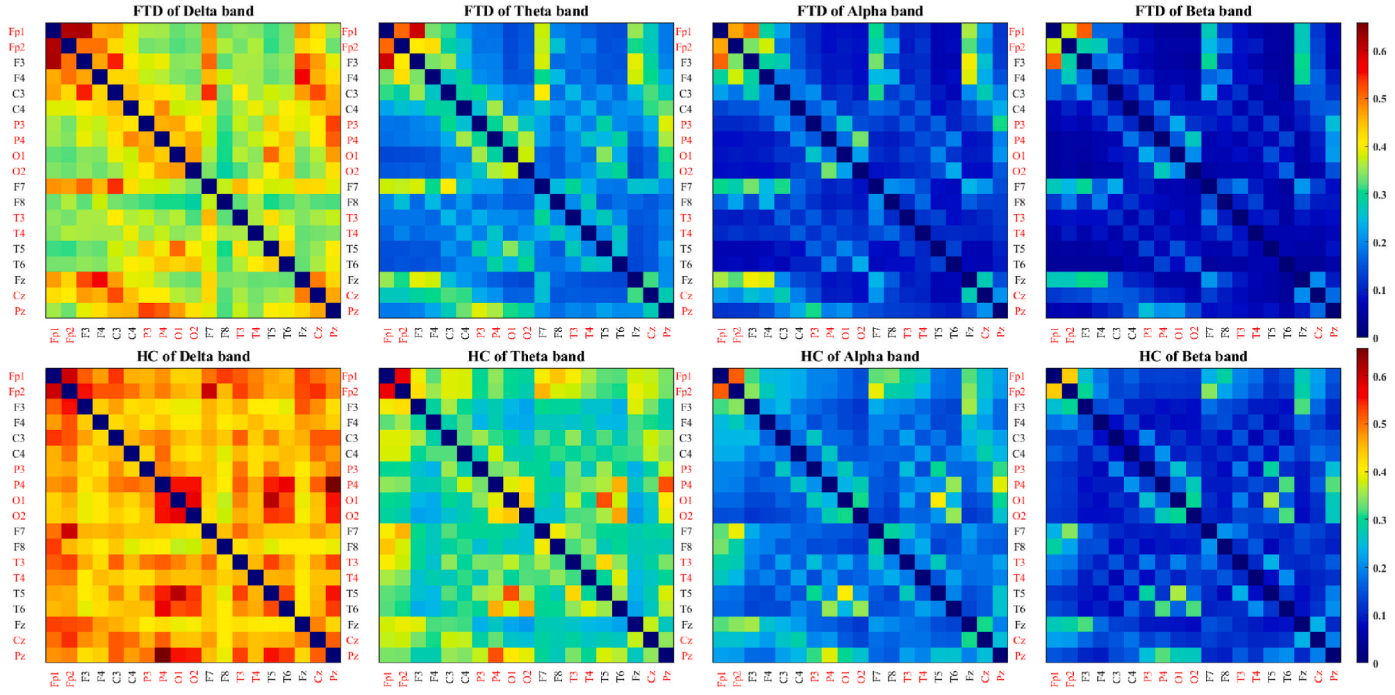

Fig. 7. MMMIFC connectivity matrix of FTD and HC in delta, theta, alpha and beta band.

Global efficiency measures the ease of parallel information transfer across the brain network, and it is defined as:

$$GE = \frac{1}{N(N-1)} \sum_{i \neq j} w_{ij} \tag{9}$$

where 'w_{ij}' denotes the edge lengths of the weighted adjacency matrix and 'N' is the number of the EEG channel, here N = 19.

Diffusion efficiency captures the capacity of the brain network for robust information flow via not only the shortest but also alternative paths. Defining the graph Laplacian $L = D - W$ with 'D' as the degree matrix, let 'L' be its Moore Penrose pseudoinverse. For any two distinct nodes 'I' and 'j', the mean first-passage time is

$$MFPT_{ij} = N\left(L_{ii} + L_{jj} - 2L_{ij}\right) \tag{10}$$

Diffusion efficiency is then the average reciprocal of these times:

$$DE = \frac{1}{N(N-1)} \sum_{i \neq j} \frac{1}{MFPT_{ij}} \tag{11}$$

Table 7
Mapping EEG channels to DMN brain areas.

EEG Channel	Anatomical Region	Associated DMN Subsystem
Fp1	Left PFC	Anterior DMN
Fp2	Right PFC	Anterior DMN
Cz	Central midline	DMN hub
P3	Left PCC	Posterior DMN
P4	Right PCC	Posterior DMN
Pz	Midline PCC	Posterior DMN
O1	Left OC	Posterior visual integration area
O2	Right OC	Posterior visual integration area
T3	Left LTC	Lateral DMN
T4	Right LTC	Lateral DMN

Reductions in diffusion efficiency in the brain network reflect the loss of redundant communication routes within the DMN.

The weighted clustering coefficient indexes how tightly nodes cluster into triads, and the equation of calculation of the clustering coefficient is shown as follow.

$$C_i = \frac{1}{k_i(k_i-1)} \sum_{u \neq v \in N(i)} (w_{iu} w_{iv} w_{uv})^{\frac{1}{3}}, CC = \frac{1}{N} \sum_{i=1}^{N} C_i \tag{12}$$

Where 'C_i' indexes the degree to node '*i*' form tightly interconnected triads, 'k_i' is the degree of node '*i*' and '*N(i)*' is the set of neighbours of node '*i*'. A lower clustering coefficient in the brain network reflects a breakdown of these local clusters within the DMN.

The following Table 8 and Fig. 8 illustrates the group-wise distributions of global efficiency, diffusion efficiency, and clustering coefficient in both AD and HC participants across the delta, theta, alpha, and beta frequency bands, highlighting topological network alterations in DMN region associated with AD.

In previous studies, graph theoretical metrics have been increasingly recognized as potential biomarkers for distinguishing AD from healthy cognitive aging. Spruyt et al. employed high-density EEG to examine the relationship between tau protein aggregation and functional connectivity in the alpha frequency band [40]. The findings revealed that increased tau deposition was associated with a decrease in the global clustering coefficient. Wu. et al. applied graph theory to EEG data to assess topological parameters, including clustering coefficient, global and local efficiency [41]. The results indicated that AD patients exhibited increased mean Phase Lag Index (PLI) values in the theta band, along with decreases in clustering coefficient, and global efficiency in the alpha band. These alterations reflect disrupted functional connectivity patterns in AD. Accordingly, the present analysis applies these graph metrics to EEG-derived brain networks to explore their potential as functional biomarkers in AD.

The current analysis builds upon these findings by examining graph metrics specifically within the DMN across multiple frequency bands. The results show that the theta band presents the most prominent group differences between AD and HC, consistent with previous studies highlighting theta-related connectivity alterations. **Among all pairwise comparisons, the AD vs HC contrast showed the largest differences in global efficiency, diffusion efficiency, and clustering coefficient, suggesting pronounced disruption of DMN network integration and segregation in AD. Theta oscillations within DMN hubs such as the hippocampus, posterior cingulate cortex, and medial prefrontal cortex are crucial for episodic memory processes; reduced theta-band coupling among these regions likely contributes to the observed declines in network metrics and aligns with the characteristic memory impairment in AD.** Consistently reduced values of all three-graph metrics in the delta and theta bands further support the presence of widespread low-frequency network disintegration in the AD group. Notably, a divergent pattern emerged in the alpha band, where diffusion efficiency was paradoxically higher in the AD group, suggesting a possible compensatory mechanism or frequency-specific alteration. Additionally, although all three metrics in the beta band were elevated in AD compared to HC, the magnitude of group differences was relatively small, indicating that beta band measures may have limited sensitivity in distinguishing AD from HC.

Table 8
Graph theory analysis between AD and HC in DMN network.

	Frequency bands	Global Efficiency	Diffusion Efficiency	Clustering Coefficient
AD	Delta	0.453 ± 0.072	0.374 ± 0.035	0.449 ± 0.073
	Theta	0.259 ± 0.071	0.297 ± 0.046	0.253 ± 0.072
	Alpha	0.157 ± 0.039	0.228 ± 0.039	0.148 ± 0.038
	Beta	0.137 ± 0.036	0.214 ± 0.037	0.126 ± 0.034
HC	Delta	0.494 ± 0.050	0.382 ± 0.026	0.491 ± 0.050
	Theta	0.310 ± 0.069	0.309 ± 0.043	0.305 ± 0.070
	Alpha	0.158 ± 0.045	0.203 ± 0.054	0.148 ± 0.046
	Beta	0.117 ± 0.066	0.197 ± 0.055	0.108 ± 0.066

5.3.3. Evaluation of brain function in FTD and HC

To investigate functional network alterations associated with FTD, graph theoretical analysis was applied to EEG-derived brain networks of FTD patients and HC, using the same methodological framework described in the previous section. Table 9 and Fig. 9 present the distributions of the same three graph theory measurements for FTD and HC groups. These results provide insight into the frequency-specific disruptions in functional integration and segregation in FTD. Comparisons across bands highlight distinct topological changes that may serve as potential biomarkers for distinguishing FTD from HC.

Wu et al. reported functional network alterations in FTD have been characterized by increases in theta band synchronization, as reflected by elevated mean PLI values, alongside enhancements in graph theoretical metrics such as node degree, clustering coefficient, global efficiency, and local efficiency [41]. In contrast, reductions in alpha band connectivity particularly decreased amplitude envelope correlation values have been accompanied by lower values across the same graph metrics, indicating frequency-specific disruptions in network integration. Unlike AD, these changes in FTD do not appear to follow a widespread regional pattern but are rather more localized.

In the present analysis, the most pronounced FTD vs HC differences were observed in the delta band, where all three DMN-derived graph metrics were substantially lower in the FTD group. Conversely, alpha- and beta-band metrics were consistently higher in FTD compared to HC, while theta-band values showed moderate reductions. This spectral profile differs from AD, where the largest differences occurred in the theta band, suggesting distinct frequency sensitivities of DMN disruption across the two disorders. The observed low-frequency decreases in global and local network organization likely reflect impaired long-range integration and segregation in FTD, whereas the high-frequency increases may indicate compensatory recruitment of alternative processing pathways or maladaptive hyper-synchronization within preserved cortical regions.

5.4. Significance of time-varying brain network analysis

Traditional brain network analysis often relies on static connectivity measures averaged over extended periods, assuming stable functional interactions among brain regions. However, brain connectivity is intrinsically dynamic, exhibiting fluctuations over short timescales. Using a sliding window approach, a series of time-resolved MMMIFC matrices can be computed, enabling the monitoring of functional connectivity evolution over time and revealing transient patterns that are undetectable with static analyses. In this study, a 30-s sliding window with a 5-s step size was adopted. As the analysis does not aim for real-time computation, computational latency per window was not a constraint. Compared with shorter windows, a 30-s segment provides sufficient oscillatory cycles in low-frequency bands including delta and theta band to yield more stable and reliable spectral and connectivity

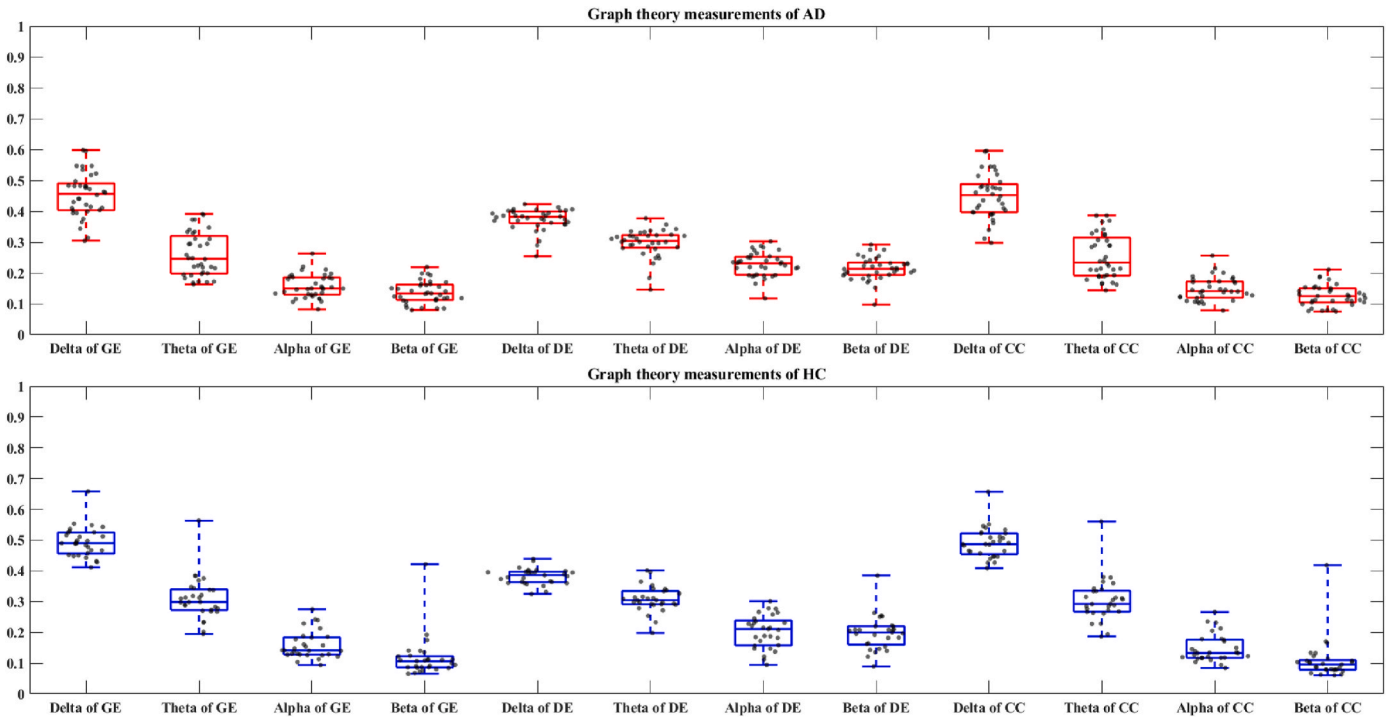

Fig. 8. Graph theory measurements of DMN brain network of AD and HC, here 'GE' is global efficiency, 'DE' is diffusion efficiency, and 'CC' is clustering coefficient.

Table 9
Graph theory analysis between AD and HC in DMN network.

	Frequency bands	Global Efficiency	Diffusion Efficiency	Clustering Coefficient
FTD	**Delta**	0.457 ± 0.087	0.367 ± 0.028	0.453 ± 0.088
	Theta	0.276 ± 0.075	0.301 ± 0.036	0.269 ± 0.073
	Alpha	0.161 ± 0.041	0.227 ± 0.045	0.151 ± 0.041
	Beta	0.139 ± 0.044	0.214 ± 0.043	0.129 ± 0.043
HC	**Delta**	0.494 ± 0.050	0.382 ± 0.026	0.491 ± 0.050
	Theta	0.310 ± 0.069	0.309 ± 0.043	0.305 ± 0.070
	Alpha	0.158 ± 0.045	0.203 ± 0.054	0.148 ± 0.046
	Beta	0.117 ± 0.066	0.197 ± 0.055	0.108 ± 0.066

estimates, while also averaging out transient noise and artifacts often present in resting-state EEG. This choice balances temporal resolution with the stability of extracted features, which is critical for robust classification.

Applying graph-theoretical metrics such as global efficiency, diffusion efficiency, and clustering coefficient to each windowed MMMIFC matrix allows characterization of the evolving topological organization of brain networks. These dynamic network features reflect the brain's flexibility and responsiveness, which are frequently compromised in neurodegenerative diseases such as AD and FTD and the detail is shown in Fig. 10.

The extracted dynamic network metrics, represented as temporal trajectories of GE, DE, and CC, serve as informative features for deep learning models. Compared to static connectivity measures, these dynamic features contain richer temporal information, enhancing the model's ability to discriminate between healthy and pathological brain states. Thus, incorporating time-varying brain network analysis not only advances the understanding of functional brain dynamics but also significantly improves the classification performance of deep learning-based diagnostic frameworks.

5.5. Limitation and contribution

Although the proposed framework demonstrates high accuracy in distinguishing AD, FTD, and HC, certain limitations remain. In particular, the current method does not achieve high sensitivity in differentiating between AD and FTD. While brain connectivity algorithms offer strong performance in distinguishing pathological from healthy states, their capability in capturing subtle differences between AD and FTD remains limited in this setting. This may reflect overlapping functional connectivity disruptions between the two disorders or the need for more discriminative features.

Moreover, the analysis employed functional connectivity measures based on MMMIFC, which do not capture the directionality of interactions between brain regions. The absence of effective connectivity analysis prevents a deeper understanding of causal or directional information flow within the brain networks, which could be critical for distinguishing between distinct neurodegenerative mechanisms.

Despite these limitations, the present study offers several key contributions. A novel deep learning–based classification approach was developed that achieves high accuracy in detecting AD and FTD from EEG data. By applying MWT, the analysis revealed that discriminative information was primarily concentrated within the 1–20 Hz frequency range. Furthermore, significant reductions in brain network function were observed in the delta and theta bands among AD and FTD patients. Specifically, the most pronounced difference between AD and HC was detected in the theta band, while the largest distinction between FTD and HC occurred in the delta band.

Additionally, the use of a sliding window technique enabled the extraction of time-varying network metrics, capturing the full temporal evolution of features such as global efficiency, diffusion efficiency, and clustering coefficient during the resting-state period. This dynamic analysis provides a more comprehensive representation of brain function and enhances the interpretability and classification power of the proposed model.

6. Conclusion

This study provided important insights into the neurophysiological distinctions between AD, FTD, and healthy aging by leveraging EEG-based functional connectivity. By identifying specific frequency bands

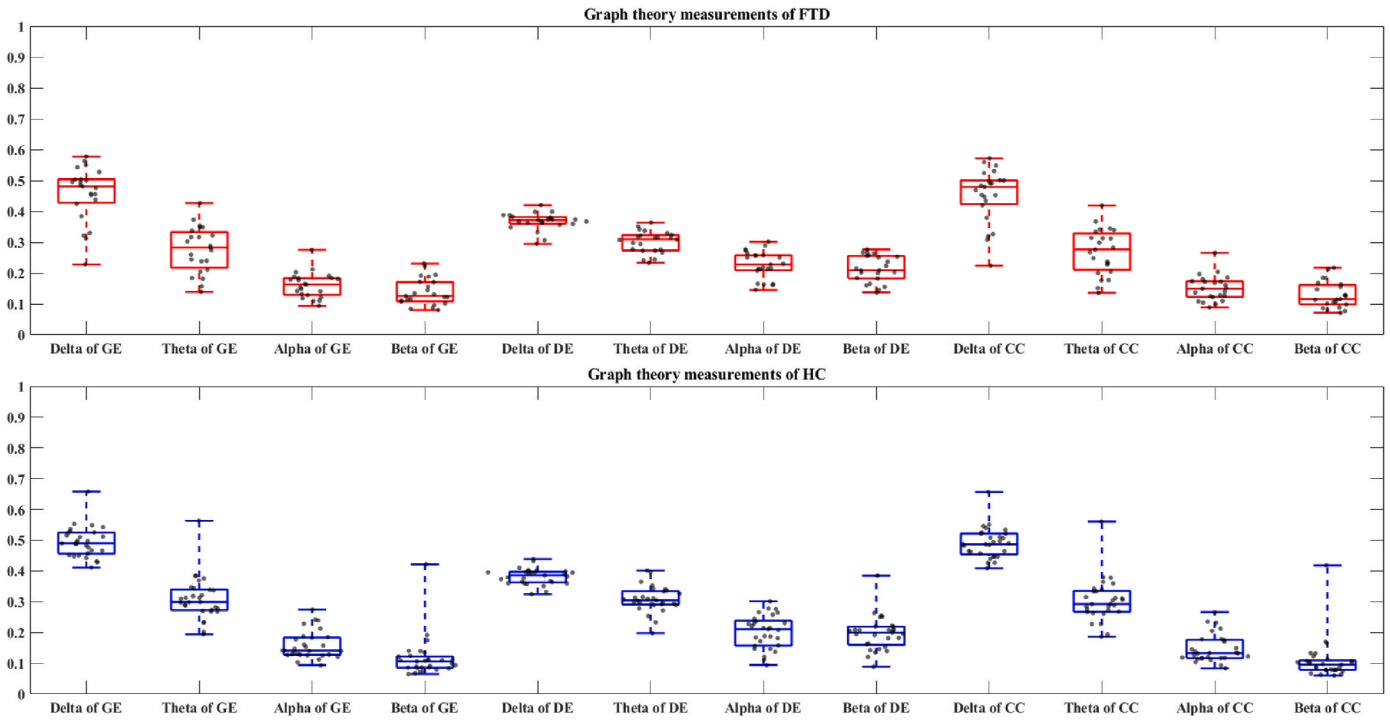

Fig. 9. Graph theory measurements of DMN brain network of FTD and HC, here 'GE' is global efficiency, 'DE' is diffusion efficiency, and 'CC' is clustering coefficient.

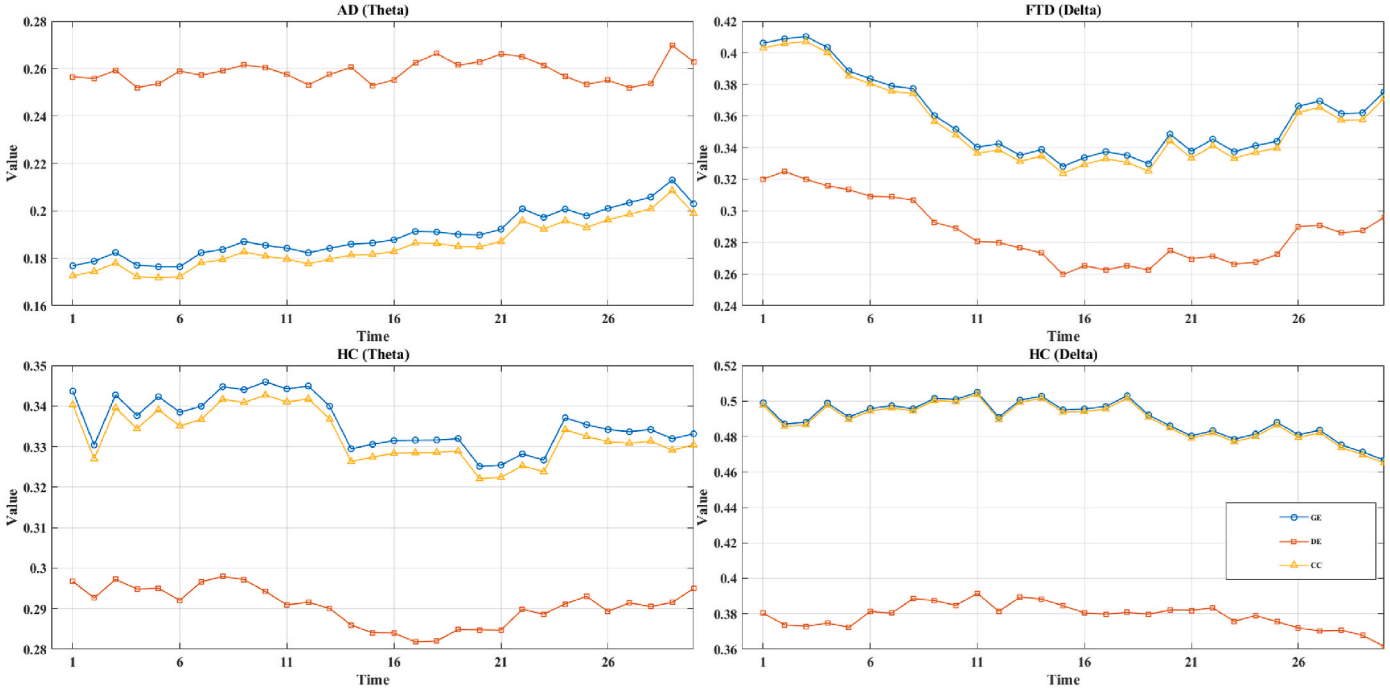

Fig. 10. Time-varying graph theory measurements in AD, FTD and HC subjects, here 'GE' is global efficiency, 'DE' is diffusion efficiency, and 'CC' is clustering coefficient.

and network alterations that differentiate these conditions, the research advanced our understanding of their underlying brain mechanisms. Importantly, the ability to extract robust biomarkers from non-invasive EEG data offered a promising avenue for earlier and more accurate diagnosis, which was crucial for effective intervention and personalized treatment. The integration of advanced connectivity metrics with deep learning paves the way for practical clinical applications, potentially improving patient outcomes and informing future dementia research.

CRediT authorship contribution statement

Mingkan Shen: Writing – original draft, Visualization, Validation, Supervision, Software, Resources, Project administration, Methodology, Investigation, Formal analysis, Data curation, Conceptualization. **Peng Wen:** Writing – review & editing, Supervision. **Bo Song:** Writing – review & editing. **Yan Li:** Writing – review & editing, Supervision.

Ethics in publishing statement

This research presents an accurate account of the work performed, all data presented are accurate and methodologies detailed enough to permit others to replicate the work.

This manuscript represents entirely original works and or if work and/or words of others have been used, that this has been appropriately cited or quoted and permission has been obtained where necessary.

This material has not been published in whole or in part elsewhere.

The manuscript is not currently being considered for publication in another journal.

That generative AI and AI-assisted technologies have not been utilized in the writing process or if used, disclosed in the manuscript the use of AI and AI-assisted technologies and a statement will appear in the published work.

That generative AI and AI-assisted technologies have not been used to create or alter images unless specifically used as part of the research design where such use must be described in a reproducible manner in the methods section.

All authors have been personally and actively involved in substantive work leading to the manuscript and will hold themselves jointly and individually responsible for its content.

Declaration of competing interest

The authors declare that they have no known competing financial interests or personal relationships that could have appeared to influence the work reported in this paper.

References

[1] D.J. Selkoe, J. Hardy, The amyloid hypothesis of Alzheimer's disease at 25 years, EMBO Mol. Med. 8 (6) (2016) 595–608.
[2] C.R. Jack Jr., et al., NIA-AA research framework: toward a biological definition of Alzheimer's disease, Alzheimer's Dementia 14 (4) (2018) 535–562.
[3] C. Babiloni, et al., Cortical sources of resting state EEG rhythms are related to brain hypometabolism in subjects with Alzheimer's disease: an EEG-PET study, Neurobiol. Aging 48 (2016) 122–134.
[4] J. Dauwels, et al., A comparative study of synchrony measures for the early diagnosis of Alzheimer's disease based on EEG, Neuroimage 49 (1) (2010) 668–693.
[5] K.D. Neylan, B.L. Miller, New approaches to the treatment of frontotemporal dementia, Neurotherapeutics 20 (4) (2023) 1055–1065.
[6] J. Bang, S. Spina, B.L. Miller, Non-Alzheimer's dementia 1: frontotemporal dementia, Lancet (London, England) 386 (10004) (2015) 1672.
[7] G. Musa, et al., Alzheimer's disease or behavioral variant frontotemporal dementia? Review of key points toward an accurate clinical and neuropsychological diagnosis, J. Alzheim. Dis. 73 (3) (2020) 833–848.
[8] A. Gifford, et al., Biomarkers in frontotemporal dementia: current landscape and future directions, Biomarkers Neuropsychiatr. 8 (2023) 100065.
[9] M. Pievani, et al., Functional network disruption in the degenerative dementias, Lancet Neurol. 10 (9) (2011) 829–843.
[10] J. Cao, et al., Ultra-high-resolution time-frequency analysis of EEG to characterise brain functional connectivity with the application in Alzheimer's disease, J. Neural. Eng. 19 (4) (2022) 046034.
[11] H. Zheng, et al., Time-frequency functional connectivity alterations in Alzheimer's disease and frontotemporal dementia: an EEG analysis using machine learning, Clin. Neurophysiol. 170 (2025) 110–119.
[12] E. Bullmore, O. Sporns, Complex brain networks: graph theoretical analysis of structural and functional systems, Nat. Rev. Neurosci. 10 (3) (2009) 186–198.
[13] K.J. Friston, Functional and effective connectivity: a review, Brain Connect. 1 (1) (2011) 13–36.
[14] W.W. Seeley, et al., Neurodegenerative diseases target large-scale human brain networks, Neuron 62 (1) (2009) 42–52.
[15] M.D. Greicius, et al., Functional connectivity in the resting brain: a network analysis of the default mode hypothesis, Proc. Natl. Acad. Sci. USA 100 (1) (2003) 253–258.
[16] X. Miao, et al., Altered connectivity pattern of hubs in default-mode network with Alzheimer's disease: an granger causality modeling approach, PLoS One 6 (10) (2011) e25546.
[17] Y. LeCun, Y. Bengio, G. Hinton, Deep learning, Nature 521 (7553) (2015) 436–444.
[18] Y. Roy, et al., Deep learning-based electroencephalography analysis: a systematic review, J. Neural. Eng. 16 (5) (2019) 051001.
[19] A. Miltiadous, et al., A dataset of scalp EEG recordings of Alzheimer's disease, frontotemporal dementia and healthy subjects from routine EEG, Data 8 (6) (2023) 95.
[20] A. Miltiadous, et al., DICE-net: a novel convolution-transformer architecture for Alzheimer detection in EEG signals, IEEE Access 11 (2023) 71840–71858.
[21] H. Zheng, X. Xiong, X. Zhang, Multi-threshold recurrence rate plot: a novel methodology for EEG analysis in Alzheimer's disease and frontotemporal dementia, Brain Sci. 14 (6) (2024) 565.
[22] K. AlSharabi, et al., EEG-based clinical decision support system for Alzheimer's disorders diagnosis using EMD and deep learning techniques, Front. Hum. Neurosci. 17 (2023) 1190203.
[23] U. Lal, A.V. Chikkankod, L. Longo, A comparative study on feature extraction techniques for the discrimination of frontotemporal dementia and Alzheimer's disease with electroencephalography in resting-state adults, Brain Sci. 14 (4) (2024) 335.
[24] X. Zheng, et al., Diagnosis of Alzheimer's disease via resting-state EEG: integration of spectrum, complexity, and synchronization signal features, Front. Aging Neurosci. 15 (2023) 1288295.
[25] Y. Ma, J.K.S. Bland, T. Fujinami, Classification of Alzheimer's disease and frontotemporal dementia using electroencephalography to quantify communication between electrode pairs, Diagnostics 14 (19) (2024) 2189.
[26] R. Wang, et al., Automatic detection of Alzheimer's disease from EEG signals using an improved AFS–GA hybrid algorithm, Cognitive Neurodynam. 18 (5) (2024) 2993–3013.
[27] M.L. Vicchietti, et al., Computational methods of EEG signals analysis for Alzheimer's disease classification, Sci. Rep. 13 (1) (2023) 8184.
[28] S. Ranjan, L. Kumar, Exploring brain network organization in alzheimer disease and frontotemporal dementia: a crossplot transition entropy approach, arXiv preprint arXiv:2409.16823 (2024).
[29] A. Al-Ezzi, et al., Disrupted brain functional connectivity as early signature in cognitively healthy individuals with pathological CSF amyloid/tau, Commun. Biol. 7 (1) (2024) 1037.
[30] M. Shen, et al., Automatic identification of schizophrenia based on EEG signals using dynamic functional connectivity analysis and 3D convolutional neural network, Comput. Biol. Med. 160 (2023) 107022.
[31] M. Shen, et al., Detection of alcoholic EEG signals based on whole brain connectivity and convolution neural networks, Biomed. Signal Process Control 79 (2023) 104242.
[32] C.A. Chetty, et al., EEG biomarkers in Alzheimer's and prodromal Alzheimer's: a comprehensive analysis of spectral and connectivity features, Alzheimers Res. Ther. 16 (1) (2024) 236.
[33] M. Rostamikia, Y. Sarbaz, S. Makouei, EEG-Based classification of Alzheimer's disease and frontotemporal dementia: a comprehensive analysis of discriminative features, Cognitive Neurodynam. 18 (6) (2024) 3447–3462.
[34] M. Acharya, et al., EEGConvNeXt: a novel convolutional neural network model for automated detection of Alzheimer's disease and frontotemporal Dementia using EEG signals, Comput. Methods Progr. Biomed. 262 (2025) 108652.
[35] M.E. Raichle, et al., A default mode of brain function, Proc. Natl. Acad. Sci. USA 98 (2) (2001) 676–682.
[36] M.D. Greicius, et al., Default-mode network activity distinguishes Alzheimer's disease from healthy aging: evidence from functional MRI, Proc. Natl. Acad. Sci. 101 (13) (2004) 4637–4642.
[37] J. Zhou, et al., Divergent network connectivity changes in behavioural variant frontotemporal dementia and Alzheimer's disease, Brain 133 (5) (2010) 1352–1367.
[38] D. Mantini, et al., Electrophysiological signatures of resting state networks in the human brain, Proc. Natl. Acad. Sci. 104 (32) (2007) 13170–13175.
[39] M.E. Raichle, The brain's default mode network, Annu. Rev. Neurosci. 38 (1) (2015) 433–447.
[40] L. Spruyt, et al., EEG-based graph network analysis in relation to regional tau in asymptomatic Alzheimer's disease, Brain Commun. 7 (2) (2025) fcaf138.
[41] S. Wu, et al., Changes of brain functional network in Alzheimer's disease and frontotemporal dementia: a graph-theoretic analysis, BMC Neurosci. 25 (1) (2024) 30.